

OVERVIEW OF THE SELF-ILLUMINATION EFFECT APPLIED TO PRESSURE SENSITIVE PAINT APPLICATIONS

Yves Le Sant
Onera
BP 72, 92322 Châtillon Cedex, France

ABSTRACT

The so-called "Self-Illumination Effect" (SI) is described. It appears when using luminescent paints like PSP. Correcting SI requires to address several problems: the paint emission model, the paint reflection model and the design of an appropriate algorithm. The emission and reflection models of a pyren-based paint are described. It comes out that the simplest model, which is the Lambertian model, matches quite well the calibration measurements made with a BRDF calibration rig. An algorithm has been implemented in the Onera's PSP software. It includes a new approach to decrease the size of the problem, which is based on the segmentation of the image in triangles. The algorithm handles the occlusions and can be used for wind-tunnel applications with an acceptable time penalty. It has been extended for real paint models. It provides a significant accuracy improvement, which is small compared to the computational effort. This leads to check the benefit of using a real model, especially for PSP applications, where the intensity method compensates for remaining errors.

INTRODUCTION

The accuracy of a PSP^{1,2,3} system depends on many factors. The accuracy of the image alignment^{4,5,6,7} and the temperature^{1,2} are the most important among them. However, there is a secondary source of effort that could have a significant effect: reflection of light. The camera is viewing at a given point and it collects light emitted by this point. All the other points of the test article emit light in every direction, including toward the viewed point (see Fig. 1). The point is lighted and it reflects a part of the incoming lights according to the paint reflection properties.

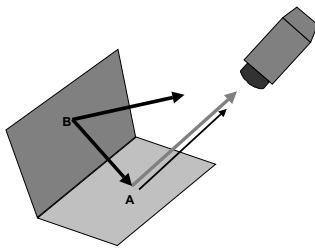


Fig. 1: the reflection effect.

All the incoming lights come from the model surface, so the reflection effect is called "self-illumination" effect. It is called SI hereafter.

Correcting the SI effect is rather difficult because SI embedded several problems, which are described in the following section. Besides, SI appears only on detailed models of real aircrafts. These models are usually quite large and are tested in large facilities. As a result, SI correction is required for industrial applications, whereas there is no need for research tests of for tests in wind tunnels of intermediate size. This may explain why there only a few papers^{8,9,10,11} about SI correction. Moreover, most of them were written by the same author Wim Ruyten^{8,9,10}.

Two sections of this paper present the emission model and the reflection model of the paint. One major difficulty of SI correction is the large size of the problem. A section details how it is handle in the Onera's software. Two sections describe how the diffuse model and the real model are implemented. A simple application using a corner is discussed.

THE EMBEDDED PROBLEMS

The usual PSP data reduction is based on the Stern-Volmer Law:

$$\frac{I_{ref}}{I} = A + B \frac{p}{p_{ref}}$$

where I_{ref} is the measured intensity at the reference pressure p_{ref} , which is often the ambient pressure. The B coefficient comes in the range 0.1-0.3, depending on the used paint. Image processing tools are involved in data reduction because the ratio I_{ref}/I requires an accurate image alignment. Softwares that performs these actions are known as resection softwares^{4,5}. Making the data reduction fully automated is a great challenge and it makes the resection softwares rather large. SI introduces new difficult problems.

The embedded problems are presented according to the way the light is emitted and measured. They are:

- + The emission model of the paint. The emission depends on the emission angle and its model must be identified.
- + The reflection model of the paint. The reflection depends on the angle of the incoming light and on the angle of the outgoing reflection.

- + The algorithm for the SI correction. It has to handle multiple reflections and this is an inverse problem. Occlusions must be considered.
- + The size of the problem. Every pixel may be lighted by all the others, leading to a huge amount of computation, which is not acceptable for nearly real time data reduction. Therefore the size of the problem must be reduced.

These problems connect the PSP data reduction to the image rendering field. They are addressed in the following sections. They are illustrated with an example obtained with the B1 paint from Optrod. This paint is illuminated with UV light and it includes a derived pyren dye and a reference dye. The pyren dye emits a blue color (500nm) and the reference dye emits a red color (620nm).

EMISSION MODEL

In order to get an idea of what could be the emission model of a PSP paint, let us consider two positions of a camera looking on a PSP sample (see Fig. 2). The former is along the vertical axis and the later is along a line making an angle θ with respect to the vertical axis. Let us assume that the length of the viewed surface is l_0 when the camera is along the vertical axis. The length l_θ related to the angle θ is then:

$$l_\theta = \frac{l_0}{\cos(\theta)}$$

Now let us assume that the concentration of the luminescent dye is uniform in the paint and that there is no light absorption. If the refraction index is assumed to be equal to 1, then it comes out that the emitted intensity $I_{e\theta}$ is proportional to the viewed length:

$$I_{e\theta} = \frac{I_{e0}}{\cos(\theta)}$$

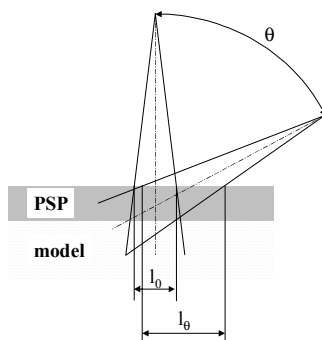


Fig. 2: emission depending on the emission angle.

This looks quite surprising because it tells that the emitted intensity increases when the emitting angle increases. This was compared to experiments that were done with a simple calibration device (see Fig. 3). A PSP sample is mounted on a rotating device and is lighted by a fiber optic, which moves as the sample. This ensures that the illumination does not

change when the angle of the PSP sample is modified. The camera is aligned to keep the center of the sample in the middle of the image.

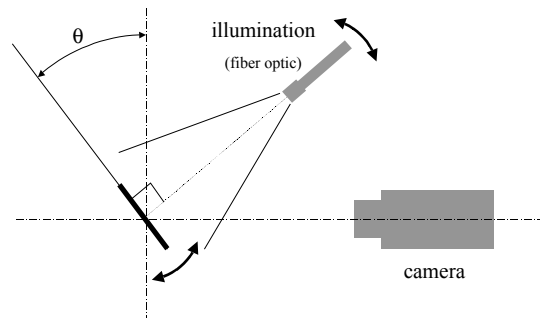


Fig. 3: calibration of the emission.

Measurements were made on several PSPs, including the B1 paint. The samples were square plates (100x100mm²) with four holes drilled near the corners. They were used during data reduction to identify the position of the camera. The identification was made for initial position ($\theta=0$). For the other positions, the images were aligned on the initial position using the Onera's resection software⁵. The images show that the emitted intensity looks nearly constant (see Fig. 4).

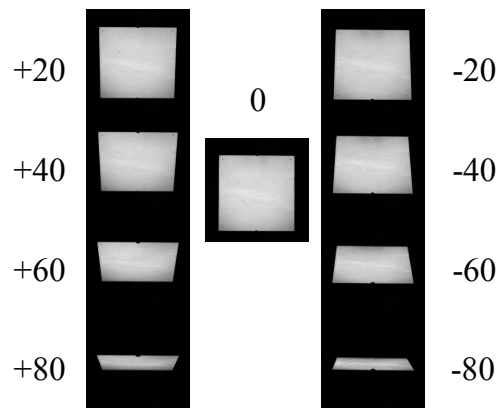


Fig. 4: emission calibration images.

A quantitative calibration of the paint was made using an average on the central line of the sample (see Fig. 5). The emission looks nearly constant and drops down significantly only over 70°.

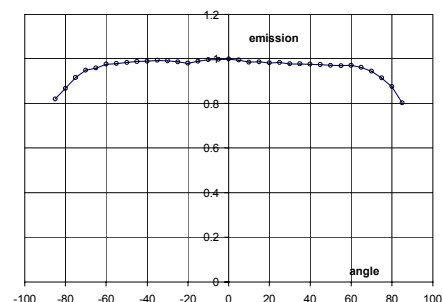


Fig. 5: emission calibration of the B1 paint.

The B1 paint behaves nearly as a Lambertian paint. This result does not agree with the simple model already presented. So the model was improved:

- + Taking into account the light absorption in the paint.
- + Modeling the reflection on the screen layer with a Lambertian model.
- + Modeling the transmission of the light through the surface of the paint by using a realistic reflection index and by applying the Fresnel's laws.

All these improvements led to the same conclusion: the emitted intensity should increase when the angle increases. This is inconsistent with the measurements so the model has to be changed. It assumes that the paint surface is without defect, which should be wrong. If the model surface is assumed to be a diffuse surface, it comes out that the emitted intensity should be constant, which agrees pretty well with the measurements. The slight decrease at high angle could be easily modeled using the generalized Lambertian model¹².

The B1 sample was covered with a thin layer of talc, which is recommended to enhance the diffuse properties of the paint. The B1 sample was also calibrated without talc and the comparison (see Fig. 6) demonstrates that a thin layer of talc improves the diffuse properties at high angle.

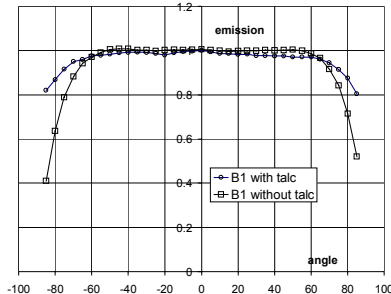


Fig. 6 : effect of talc on the emission calibration.

REFLECTION MODEL

The reflection model of the paint is the second important information required to correct the SI effect. There are two limit models: the Lambertian model (which is also called the diffuse model) and the specular model. These two models are presented hereafter, then the real model of the B1 paint is discussed.

The Lambertian model

The Lambertian model states that the incoming light is reflected in every direction and that the reflected intensity depends only on the angle between the reflected direction and the normal vector (see Fig. 7).

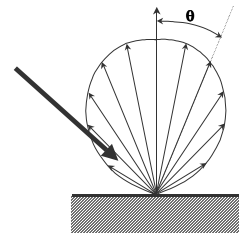


Fig. 7: the Lambertian model.

The Lambertian model is easy to handle and this is the reason why it is widely used in image rendering¹². The Lambertian law is:

$$I_r = I \frac{R}{\pi} \cos(\theta)$$

where I is the incoming light and I_r is the reflected light. R is the diffuse reflection factor and is lower than 1. R is also known as the albedo factor. The collected light does not change when looking at a diffuse body. This is because the cosine decrease is compensated by the increase of the viewed area (see Fig. 2). A good example of a diffuse surface is the Moon: it looks flat, whereas it is a sphere.

The specular model

The specular model works as a mirror: the incoming energy is reflected in the opposite direction (see Fig. 8). It looks simple but is difficult to handle because the direction of the incoming light must be taken into account when computing the reflected light.

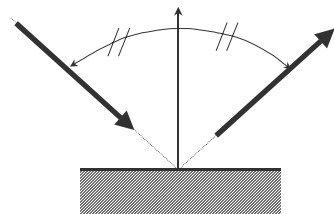


Fig. 8: the specular model.

A reflection calibration rig

The reflection models are calibrated in a BRDF calibration rig. BRDF means Bidirectional Reflectance Distribution Function. The reflected energy is given by the relation:

$$I_r = I \frac{BRDF(\theta)}{\pi} \cos(\theta)$$

where the BRDF function depends on the incoming direction and on the reflected direction. A uniform BRDF is obtained for a Lambertian paint. A BRDF calibration rig¹³ includes a lamp for the emission and a spectrometer to measure the reflected light on the sample (see Fig. 9). The lamp emits white light, enabling to calibrate the BRDF function in the visible range. The emission lamp moves from 0 to 60° (see Fig. 10, 0 is the vertical position). The zenith angle of the spectrometer moves from 0 to 60° and the

azimuth angle moves from 0 to 180° (180° is in the opposite direction of the emission as in Fig. 9).

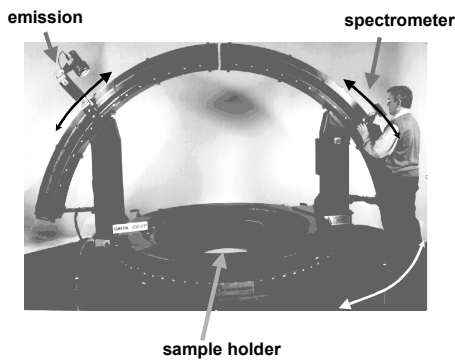


Fig. 9: the Onera's BRDF calibration rig.

This calibration rig is large because it is used to calibrate BRDFs for ground materials as sand, grass, concrete, etc... These BRDFs are used for observation from satellite, typically to track natural resources.

The BRDF of the B1 paint

The B1 paint, used with talc, was calibrated in the Onera's BRDF calibration rig (see Fig. 11). The BRDF looks nearly Lambertian when the zenith angle of illumination is 10°, while a specular reflection

appears when the zenith angle increases. The maximum value is always obtained in the specular direction as the usual. The low value obtained for the azimuth value of 0° is wrong because the spectrometer is in front of the lamp and the PSP sample is no longer illuminated.

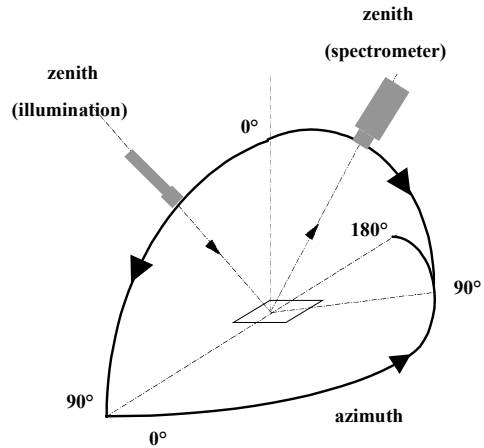


Fig. 10: zenith and azimuth angles in the BRDF calibration rig.

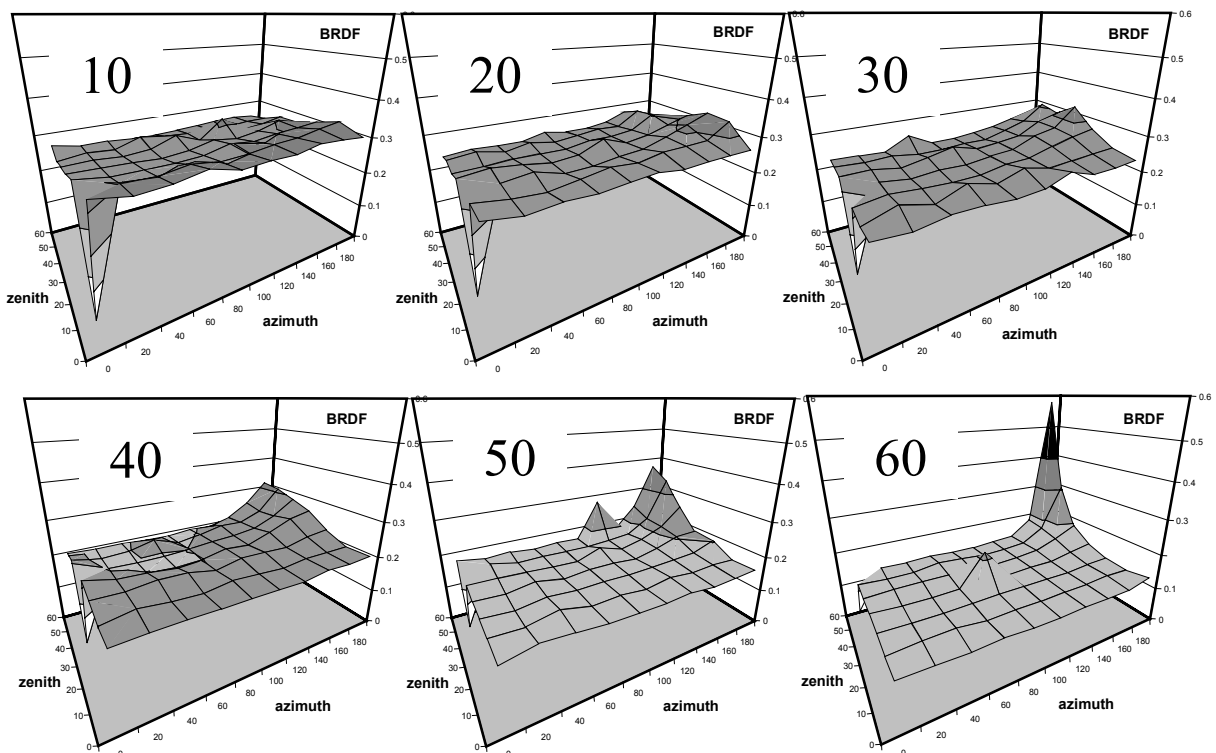


Fig. 11: the measured BRDF of the B1 paint (versus the illumination zenith angle).

The measured BRDF looks like the sum of a diffuse model and of a specular model. The specular feature appears clearly for the angle 60°, where a specular peak is observed, as well as a

secondary peak at the azimuth angle 90°. The value of the diffuse reflection factor depends on the zenith angle of illumination, so a generalized Lambertian model¹² should be used. This model

replaces the cosine function by a function of the cosine. It can be expressed as:

$$I_r = I \frac{R}{\pi} f(\cos(\theta))$$

Modeling the specular feature of the measured BRDF is more complicated and requires to use a more sophisticated model, as the Phong model .

The Phong model

The Phong model¹⁴ is the sum of a Lambertian model and of a specular model. Its expression is:

$$BRDF(\alpha) = k_d + k_s \frac{n+2}{2} \cos^n(\alpha)$$

where α is the angle between the specular direction and the reflected direction. There are three constants:

- + k_d represents the diffuse model.
- + k_s represents the specular model.
- + n is used to sharpen the specular peak: high values of n provide a fine and intense peak.

The Phong model is widely used in image rendering since it is not too complicated while it provides realistic images. Some improvements

have been done to make it more suitable for real materials¹⁵. One interesting feature of the Phong model is that k_s represents the total energy of the specular reflection. Then the sum k_d+k_s must be lower than one to ensure that the reflected energy is lower than the incoming energy. High values for the parameter n are used to obtain thin peak (see Fig. 12).

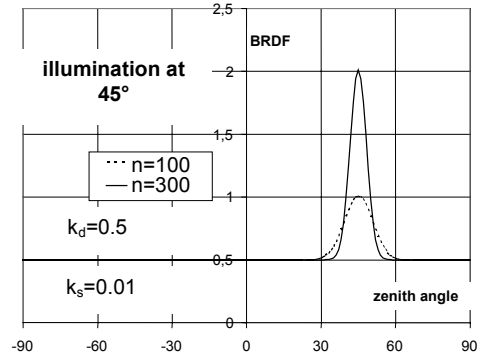


Fig. 12: BRDF of the Phong model.

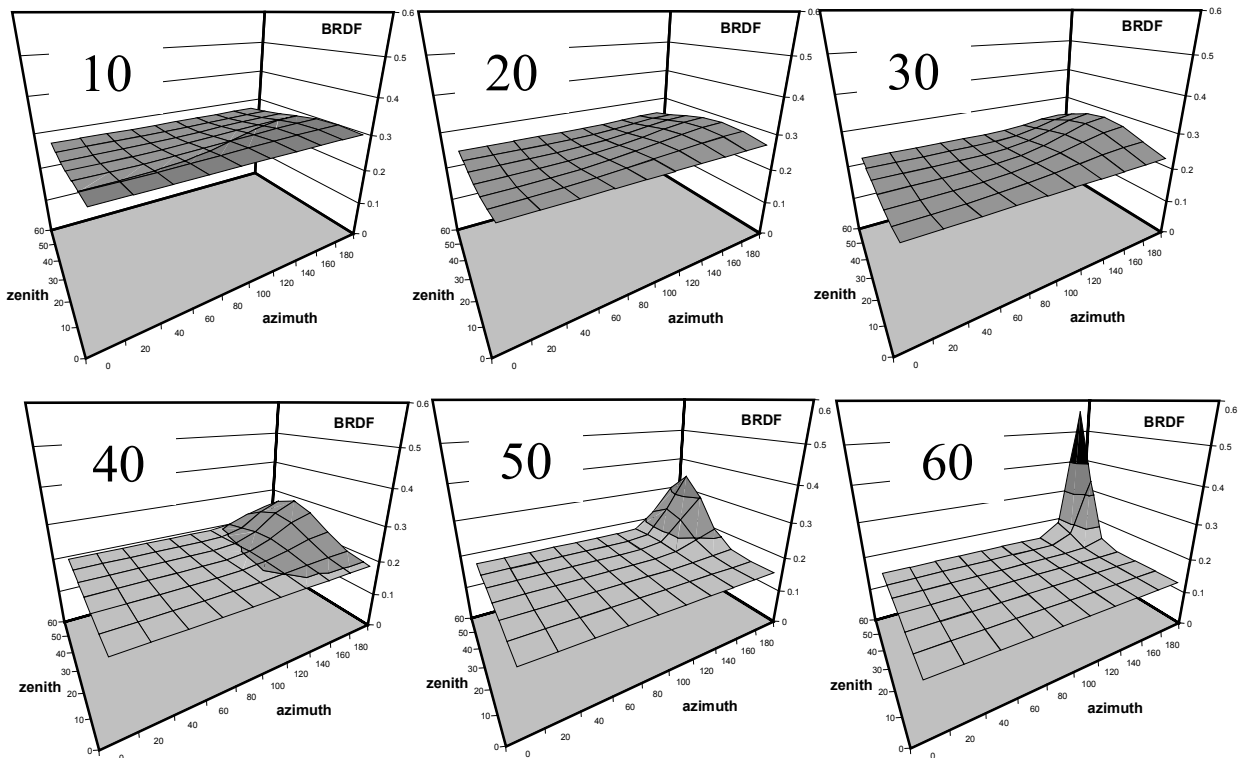


Fig. 13: the modeled BRDF of the B1 paint.

The BRDF model for the B1 paint

The proposed model is a modified Phong model. From the results presented in Fig. 11, it seems that most of the reflected energy is in the diffuse reflection, but the diffuse parameter k_d depends on the zenith angle of the illumination. The peak of the specular reflection becomes thinner when the zenith

angle increases. This suggests to increase the value of the parameter n of the Phong model.

Preliminary computations were done to assess the optimized values of the parameters k_d , k_s and n of the Phong model for each value of the zenith angle. Then these values were drawn versus the zenith angle and

were used to adjust a function. The modified Phong model for the B1 paint is then:

$$BRDF(z_i, \alpha) = k_d(z_i) + k_s(z_i) \frac{n(z_i) + 2}{n(z_i)} \cos^n(z_i)(\alpha)$$

where:

$$k_d(z_i) = 0.291 - 0.143 z_i$$

$$k_s(z_i) = 0.012 + 0.004 z_i$$

$$n(z_i) = \frac{5.25}{\cos(z_i)^{3.21}}$$

The zenith angle z_i of the illumination is expressed in radian in these equations. The standard deviation of this model is 0.006, which is roughly 3% of the average diffuse reflection factor.

The results of the model (see Fig. 13) can be compared with the measured model (see Fig. 11). Two improvements could be made:

- + The model does not take into account the secondary peak that appears at 50° and 60°.
- + The specular peak could be broadened toward the high value of the zenith angle (see 40° and 50°). It would be interesting to introduce an asymmetric effect for the specular reflection.

These improvements could be made providing a refined calibration is available. The azimuth step and the zenith step should be 5°, and it would be very useful to reach 70° for the zenith angle instead of 60°. However this limit is difficult to overcome since there are limitations for the PSP sample. This would induce a modification of the viewing angle of the spectrometer to ensure that it is looking on the sample. For example, the calibration images of the emission (see Fig. 4) show that the visible part of the sample decreases drastically over 70°.

The ratio k_s/k_d is the ratio between the energy in the specular reflection and in the diffuse reflection. Its value is 5% at angle 0 (top illumination) and 12% at 60°. An average value at 45° is 9%. This means that the energy in the specular reflection is small compared to the energy in the diffuse reflection. Then it can be stated that the B1 paint behaves as a diffuse surface.

Equivalence of the diffuse model and the specular model

The diffuse model and the specular model are the limits of BRDF models. They can be easily distinguished in real life, but there are cases where they produce the same result. Let us consider a corner made with two plates 1 and 2, which emit uniform energy I_1 for the plate 1 and I_2 for the plate 2 (see Fig. 14). The camera is looking at a point A on the plate 1, with an angle θ with respect to the normal to the surface 2.

Let us consider the case of the Lambertian model. Assuming that the two plates are very large, or that the point A is close to the plate junction, it can be

demonstrated that the point A receives the energy $0.5I_2$ from the plate 2. Then the total emission is $I_1 + 0.5I_2$ and the camera receives the energy $I_1 + 0.5I_2$, according to the Lambertian model.

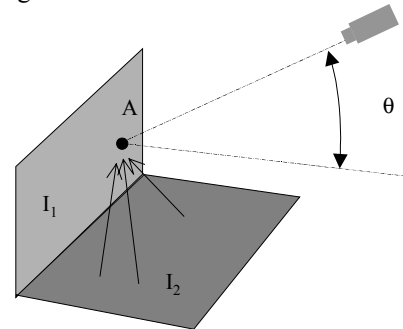


Fig. 14: the case of the corner (Lambertian model).

Now let us consider the case of the specular model (see Fig. 15). The camera looks on the point A and receives a specular reflection from the point B. This point is seen as the point B', which is the mirror image of the point B. According to the Lambertian emission model, the image point B' emits the energy I_2 toward the camera. The energy received by the camera is then $I_1 + I_2$.

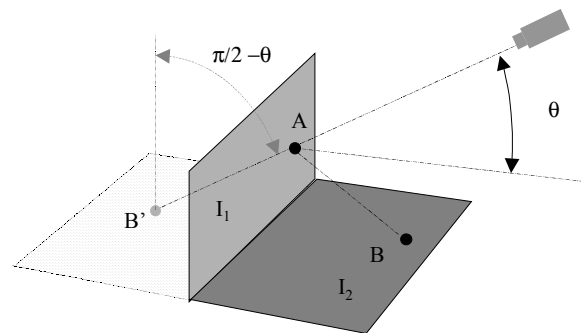


Fig. 15 : the case of the corner (specular model).

This leads to the following remark: if the energy of the plate 2 is I_2 in the case of the diffuse reflection model and if the energy of the plate 2 is $I_2/2$ in the case of the specular reflection model, the camera will collect the same energy in both cases. An observer cannot make the difference between them without extra information.

The corner geometry is a case where the diffuse model and the specular model are nearly equivalent. This surprising result is useful for the practical use of PSP. For instance, the corner case appears in regions where the pressure is nearly uniform. It is expected that regions where there is a shock wave are the only cases where a significant discrepancy can be observed between the diffuse and the specular model.

THE SIZE OF THE PROBLEM

Every point on the model may be affected by a SI effect. When considering the image, this means that

every pixel may reflect the light coming from all the pixels of the image. Therefore all the possible interactions have to be checked. SI correction algorithms comprise several steps and the two first ones are:

- + Check if a pixel can see another one. This is the occlusion problem.
- + Calculate interaction coefficients.

If the size of the image is 1000x1000, there are 10^6 pixels and the occlusion problem leads to 10^{12} operations. Assuming that a pixel is affected by less than 10% of all the other pixels, the assessment of the interaction coefficients leads to 10^{11} operations.

These amount of operations are extremely large, and this is the reason why image rendering is so time consuming (several hours of computation may be required for intricate scenes). This is not acceptable for wind tunnel application made nearly in real time, so the size of the problem must be reduced.

The first way to reduce the size of the problem is to use the grid of the model instead of the image. Usual grids for PSP applications are made of 10^5 triangles, so both the size of the occlusion problem and of the interaction coefficient computation are reduced by a factor 100 compared to the image approach. This is the solution that has been chosen in the existing published SI correction methods^{8,9,10,11}.

However, the grid solution remains rather time consuming and it requires grid with triangles of similar size. Moreover, many triangles are not seen in good conditions so their related surface on the surface may be reduced to a few pixels.

The Onera's SI correction method has been developed with a new approach, based on the image. There are two basic ideas:

- + The SI effect is observed on the image. So it is better to start from the image, not from the grid.
- + Because the size of the image is too large, it will be segmented into small areas, which are roughly triangles.

An algorithm has been designed and implemented into the Onera's resection software Afix2⁵. The main features of this algorithm are:

- + The typical size of the triangle is fixed by the user and is expressed in pixels (typically from 5 to 20).
- + A triangle gathers pixels that are on the same area on the model and where the vector normal to the surface is nearly uniform. The acceptable discrepancy with the averaged vector is fixed by the user and is typically 10° .
- + Triangles that are too small (less than 3 pixels) or too thin (straight line) are gathered within the nearest available triangle.

As a result, the segmented image is made with areas that look mainly as triangles. Fig. 16 is an example of a segmented image. The model is a corner and the two faces are clearly distinguished in the middle of the image, because there is a change in the direction of the vector normal to the surface. The right part of this figure is a zoom made on the white square.

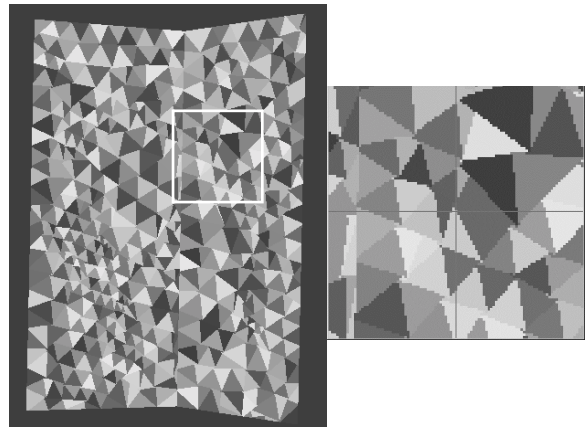


Fig. 16: segmented image.

There are usually less than 10000 areas in the segmented image (Fig. 16 comprises less than 1000 triangles to make the figure more clear). The size of the problem decreases drastically compared to the usual grid solution. There is roughly a factor 100 between the computation time required by the grid solution and by the segmented image solution.

However, decreasing the size of the problem may have an effect on the accuracy of the SI correction. For the segmentation approach, the SI correction will be interpolated on the triangle and this may introduce an error. As it has been stated by W. Ruyten¹⁰, assessing the SI effect is a compromise between the speed and the accuracy. The segmentation solution is fast and provide a good accuracy with diffuse paint.

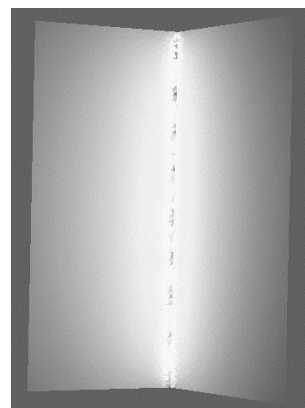


Fig. 17: the sensitivity image for the corner.

An interesting result of the segmentation method is to provide a sensitivity image. The computed interaction coefficients provide the SI effect with respect to the Lambertian model (see below). The sensitivity image

is the sum of all the interaction coefficients. It is equal to the image that would be obtained when all the points emit the same amount of light. This image would be obtained by using an uniform illumination pattern. Fig. 17 is the image obtained on a corner. The region close to the plate junction is bright, showing where are the largest SI effects. The brightness decreases at the top and at the bottom of the corner because points in these areas are less illuminated. It can be demonstrated that there is a factor 2 between the middle of the corner and the top/bottom positions. This image can be computed analytically and was used to validate the segmentation algorithm.

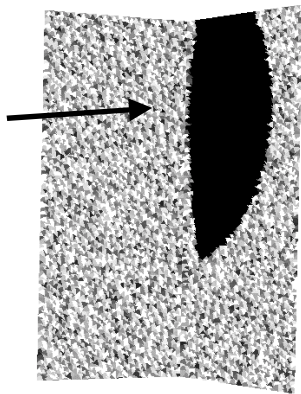


Fig. 18: viewing the interacting areas.

At last, the implementation of the algorithm enables to check for each area where are the areas that interact significantly with it. The image of the corner was segmented into 8000 triangles. Fig. 18 shows the segmented image and the arrow points on a small area while the dark region on the right plate gathered areas that interacts with the area on the left plate. The sensitivity image and the viewing tool help to get a good feeling about the possible SI effect on a model.

Computing the interaction coefficients

The segmentation algorithm divides the image in small triangles and computes their interaction coefficients, which are their relative solid angles. It is necessary to ensure that two surfaces can see each other before to calculate their interaction coefficient.

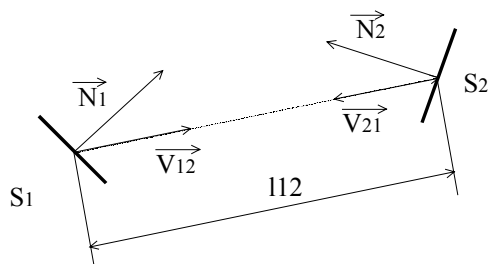


Fig. 19 : computing the interaction coefficient.

Two surfaces S_1 and S_2 (see Fig. 19) see each other if:

+ $\vec{N}_1 \vec{V}_{12}$ is positive.

+ $\vec{N}_2 \vec{V}_{21}$ is positive.

Then the interaction coefficient is:

$$A_{12} = A_{21} = \frac{\vec{N}_1 \vec{V}_{12} \vec{N}_2 \vec{V}_{21}}{\pi l_{12}^2}$$

Assuming a Lambertian reflection, with a diffuse factor R , the surface S_2 will receive the following energy from the surface S_1 :

$$A_{12} R S_2$$

THE OCCLUSION PROBLEM

Some part of the model may block the line of sight from one point to another one. This problem is a major difficulty in image rendering and is known as the occlusion problem. Checking the occlusions seems quite easy for a human operator, but it is rather difficult to design an efficient and fast algorithm that does the same as the human eye. There are many proposed solutions and the one that has been already used for SI correction is the Z-buffering technique¹⁰.

Let us describe briefly the Z-buffering technique. An hemisphere is built around a point (with the image segmentation technique, this point would be the center of a triangle). Then all the other points are checked (all the triangles). The intersection of the line going from the point to a second point with the hemisphere is calculated, and the distance to the second point is recorded. If the intersection with the hemisphere has been already obtained with a third point, then the distances of the second point and of the third point are compared. The viewed point is the one with the lower distance.

The solution implemented in Afix2 is different. It takes the advantage of the available information coming from the resection process⁵. Before to perform the segmentation of the image, the point of view of the camera must have been identified. One result of this identification process is to link every pixel to a 3D point on the model. As a consequence, the distance to the camera of every pixel (in fact, of the connected 3D point) is known. Then checking the possible occlusion is simple:

- + To check if a triangle can illuminate another one, a line between them is drawn.
- + For each pixel on this line, calculate its 3D coordinates and its distance to the camera.
- + Compare this distance to the distance provided by the resection process; the line of sight is blocked if the former distance is greater than the later.

This algorithm has been tested and validated, but was not so fast than expected. This was because there are a lot of pixels along a line so there are many checking operations. It has been slightly modified to make it faster. Pixels are replaced by triangles, so there are

less checking operations because there are less triangles on a line.

IMPLEMENTATION OF THE DIFFUSE MODEL

The interaction coefficients computed when the image is segmented are used for the diffuse model. Only the inverse algorithm is discussed here. It has been firstly described by W.Ruyten⁸, who has demonstrated that the correction is straightforward for the diffuse model.

The assumptions are:

- + The emission of the paint is Lambertian.
 - + The reflection model of the paint is Lambertian.
- The reflection factor is R.

Then, if a point emits the luminescence energy I_e and receives the energy I_i , the reflected energy will be $I_r=RI_i$. The emitted energy, including the reflected energy, will be I_e+RI_i . The important point is that the reflected energy behaves as the emitted energy, so they can be mixed without restriction.

The SI correction problem can be written using a matrix system. Let I_0 be the emitted energy, produced by the luminescence process. I_0 is a $N \times 1$ matrix where N is the number of triangles produced by the image segmentation step. This intensity is reflected on the model surface and the triangles receive the energy $R_0=AxI_0$, where A is a $N \times N$ matrix. The coefficients of A are the interaction coefficients. Then the reflected energy R_0 is also reflected and the second reflection is $R_1=AxR_0=A^2xI_0$. It comes out that the n^{th} reflection has the energy level $R_n=A^{n-1}xI_0$. The sum of the emitted light and all the reflections is the measured energy and is expressed as:

$$I_m = I_0 + AI_0 + A^2 I_0 + \dots + A^n I_0 + \dots$$

This expression can be simplified, according to W. Ruyten:

$$1 + A + A^2 + \dots + A^n + \dots = (1 - A)^{-1}$$

This expression is valid because the coefficients of the matrix A are smaller than 1, then A^n vanishes to zero. This means that reflections become less and less powerful.

The very interesting result is that the original intensity I_0 can be deduced in a single step process from the measured intensity I_m :

$$I_0 = (1 - A) I_m$$

The correction of the SI effect is then quite fast to compute. Most of the time is spent in computing the A matrix, and mostly in checking the possible occlusions.

IMPLEMENTATION OF THE REAL MODEL

The real model should be used when the reflection model includes a significant specular reflection, or when the diffuse reflection does not behave as the

emission model. For example, the BRDF model of the B1 paint, which is described in a specific section in this paper, includes a specular reflection. It has been demonstrated that the specular reflection can be neglected, but this does not mean that the diffuse model can be used. Indeed, the diffuse factor of the B1 paint depends on the reflection angle, whereas the emission factor is nearly constant. As a result, the emission and the reflection cannot be mixed and the real model should be used.

The basic idea of the implementation of the real model is to consider separately the emission and the reflection. It is an iterative algorithm. For each iteration, the main steps are:

- + Calculate the emission of each triangle toward the other triangles.
- + Add this emission to the reflection toward the other triangles; this provides the total emission.
- + Calculate the reflection of the total emission on the others triangles, by using the BRDF model.
- + Calculate the total emission toward the camera and update the emission to match the total emission and the measured emission.

The emission and the reflections are kept in memory for each triangle. The reflection coefficients are recalculated for each iteration, because it not possible to keep them in memory. For example, let us consider a case with 1000 triangles, each of them viewing 100 triangles. For each triangle, there are 100×100 reflection coefficients. There are 10^7 coefficients leading to store about 10Mb in memory. But this number grows as N^3 , so if there are 5000 triangles, the number of coefficients will be 125×10^7 , i.e. 1.25Gb!

Numerical simulation have shown that the algorithm is not stable when the specular reflection is important. Therefore, a relaxation factor must be used for difficult cases.

The implementation of the real model has been validated by using a Lambertian BRDF. In this case, the algorithm must find the right solution at the first iteration. This is because the total emission $(1+A)I_m$ toward the camera is obtained at the first iteration. The correction on the emission is then $I_m - (1+A)I_m = -AI_m$, leading to the emission $I_m - AI_m$, which is the right value.

APPLICATIONS

The corner

The corner is a good test to validate a SI correction algorithm. A corner was painted with a pyren-based paint (not the B1 paint) providing an image with a significant SI effect (see Fig. 20) near the junction of the two plates. Then the left plate was covered with a

black sheet, removing the SI effect on the right plate (right image in Fig. 20).

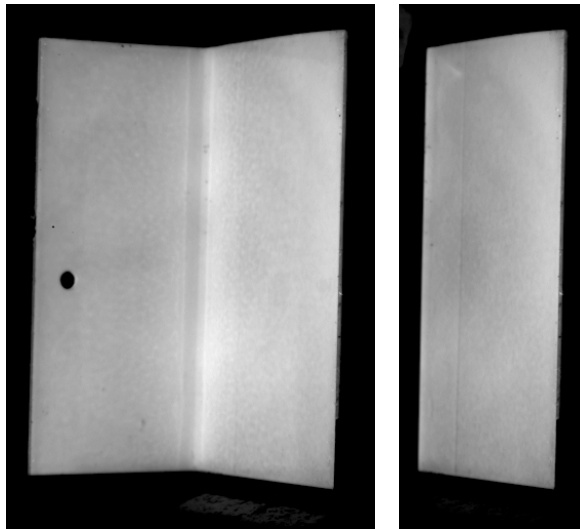


Fig. 20 : the corner test.

The SI effect is about 40% near the junction and decreases down to 15% (see Fig. 21). The BRDF of the used paint was not calibrated, but some useful information can be get from the comparison of cuts with and without SI:

- + If the paint is a diffuse paint, the SI should decrease from the junction to the border. This is because points near the junction see the left plate as a semi-infinite plane. On the other hand, the left plate does not look as a semi-infinite plane for points near the right border. Then the SI effect according to the diffuse model should decrease.
- + If the paint is a specular paint, the SI effect is nearly the same for all the points, then the curve without SI should be nearly parallel to the curve with SI.

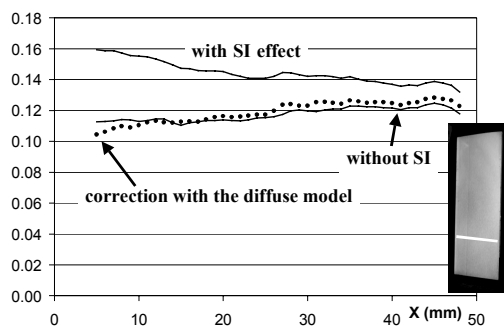


Fig. 21: correction with the diffuse model.

These two remarks lead to the conclusion that the paint behaves mostly as a diffuse paint. Moreover, if the paint is specular, it works as a mirror and the dark hole visible on the left plate should be seen on the left image. This is not the case, so this make quite sure that the paint is not specular.

As a consequence, the correction was computed by using the diffuse model, with a reflection factor R of 1. The correction is quite good (see Fig. 21), but there are some discrepancies near the right border. This could be corrected by introducing a specular part in the model, because the specular reflection will enlarge the correction for points far from the junction.

A Phong model was used as a real model. Its parameters were adjusted to obtain a good agreement with the results without SI: $k_d=0.8$ $k_s = 0.2$ $n=10$. The agreement is then very good (see Fig. 22).

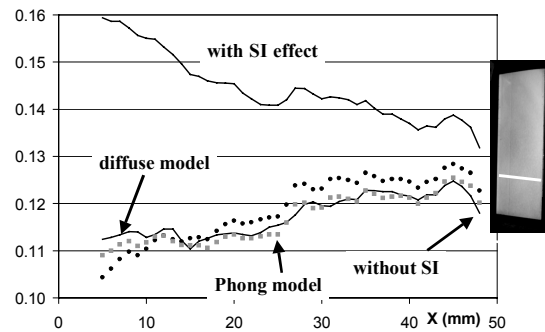


Fig. 22: correction with the diffuse and the Phong models.

Using a model that includes a specular reflection improves the accuracy, but the drawback is the computation time: the correction using the diffuse model needs roughly 1s, while the correction with a Phong model needs about 30mn!



Fig. 23: a real test.

A real test

A test was made on an aircraft model equipped with an engine (see Fig. 23). The model was painted with the B1 paint. As it has been demonstrated, the BRDF of the B1 paint is nearly diffuse but it depends on the incoming angle. An average diffuse factor of 0.25 was used as a constant diffuse factor, and the images were corrected with the diffuse model. The sensitivity image (see Fig. 24) shows that the SI effect is mainly located on the support of the engine. However, the effect is quite large on the part of the wing close to the support. The corrected image shows an effect of about 10%.

Tests were done with and without paint on the engine and its support. No difference was observed on the wing with pressure taps as well as with PSP. This is because of the ratio used in the Stern-Volmer law: the error due to SI is nearly the same on the reference image as on the test image.

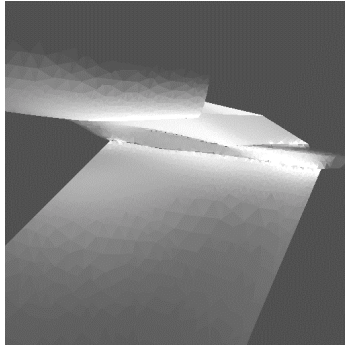


Fig. 24 : SI sensitivity image.

Unfortunately, the paint was removed from the engine without covering it with a black paint. The surface of the engine behaves as a mirror, so it was not possible to make a comparison with the corrected images.

CONCLUSION

The emission models of several paints were calibrated. They agree pretty well with the diffuse model. The BRDF model of the B1 paint was calibrated and identified. Its most important part is the diffuse model, which depends on the illuminating angle. The specular part can be omitted, since its effect is less than 10%.

A BRDF correction module has been implemented in the Onera's resection software. It uses a segmentation algorithm to decrease the size of the problem. As a result, the correction of the SI effect is very fast for diffuse models. It can be integrated into the usual data reduction process. The software can handle non-diffuse models, but the computation time increases drastically, making not possible to use it for usual PSP applications.

It is demonstrated that the diffuse model and the specular model are nearly similar for corner regions. Moreover, the Stern-Volmer law corrects itself the SI effect, so it is expected that the SI effect would be visible only when shock waves appear in the region where SI may occur. Using a paint prepared with talc will enable to use the diffuse model for the correction.

It appears that the SI problem has been solved in a useful manner, since all the problems have been solved (including the occlusion problem) and the computation time is quite low.

ACKNOWLEDGMENTS

The development of the presented SI correction module was conducted with the financial support of the French Ministry of Defense (SPAé). The author would like to thank Gerard Serrot for helping him in discovering the BRDF world.

REFERENCES

- 1). Bell, J.H., Shairer, E.T., Hand, L.A., Mehta, R.D., 2001, "Surface Pressure Measurements Using Luminescent Coatings", *Annual Review of Fluid Mechanics*, vol. 33, pp. 155-206, March.
- 2). Sullivan, J., "Temperature and Pressure Sensitive Paint", *Lecture Series 2000-2001, Advanced Measurement Techniques, Von Karman Institute for Fluid Mechanics*, January.
- 3). Buck, G.M., "Simultaneous Global Pressure and Temperature Measurement Technique for Hypersonic Wind Tunnels", 2000, *21st AIAA Aerodynamic Measurement Technology and Ground Testing Conference*, Denver, CO, 19-22 June.
- 4). Bell, J.H., McLachlan, B.G., "Image Registration for Luminescent Paint Sensors", 1993, *31st Aerospace Sciences Meeting & Exhibit*, Paper AIAA 93-0178.
- 5). Le Sant, Y., Deléglise, B., Mébarki, Y., "An Automatic Image Alignment Method Applied to Pressure Sensitive Paint Measurements", 1997, *17th ICIASF*, Monterey (U.S.A.), September 29, October 2.
- 6). Liu T, Cattafesta L.N., Radeztsky R.H., "Photogrammetry Applied to Wind-Tunnel Testing", 2000, *AIAA Journal*, Vol.38, Num 6., pp 964-971.
- 7). Ruyten, W., "Model Attitude Measurement with and Eight-Camera Pressure-Sensitive Paint System", 2000, *38th AIAA*, Reno, Nevada, paper AIAA 2000-0833, January.
- 8). Ruyten, W.M., "Correction of self-illumination and spectral-leakage effects in luminescent-paint measurements", 1997, *Applied Optics*, vol.36, n°14, pp 30793085, May.
- 9). Ruyten, W.M., Fichser, C.-J., "On the Effects of Reflected Light in Luminescent Paint Measurements", 2000, *38th AIAA*, Reno, Nevada, paper AIAA 2000-0833, January.
- 10). Ruyten, W.M., "Reconstruction of the net emission distribution from the total radiance distribution on a reflecting surface", 2001, *Journal of Optical Society of America*, vol.18, No.1, pp.216-223, January.
- 11). Morozov, A.-N., Smirnov, P.-A., "Increase of accuracy of pressure sensitive paint method by means of radiation self-illumination account", 1999, *Euromech 406 Colloquium*, Warszawa, Poland.
- 12). Oren, M., Nayar S.K., "Generalization of the Lambertian Model and Implications for Machine Vision", 1995, *International Journal of Computer Vision*, vol.14, issue 3, pp. 227-251, April.

- 13). Serrot, G., Bodilis, M., Duffaut, J., 1997, "Propriétés radiométriques des scènes", Report CERT/DERO RT 1/6426.
- 14). Phong, B. 1975, "Illumination for computer generated pictures", *Communication of the ACM*, vol18, n°6, pages 311-317.
- 15). Lafortune, E., Willems, Y., 1994, "Using the Modified Phong Reflectance Model for Physically Based Rendering", Report CW 197, Department of Computing Science, K.U. Leuven, Novembre 1994.